INTERNATIONAL JOURNAL OF CLIMATOLOGY
Int. J. Climatol. (2016)
Published online in Wiley Online Library
(wileyonlinelibrary.com) DOI: 10.1002/joc.4917

RMetS
Royal Meteorological Society

Characteristics of mesoscale convective systems in central East China and their reliance on atmospheric circulation patterns

Zhiwei He,[a] Qinghong Zhang,[a,b]* Lanqiang Bai[a] and Zhiyong Meng[a]

[a] *Laboratory for Climate and Ocean-Atmosphere Studies, Department of Atmospheric and Oceanic Sciences, School of Physics, Peking University, Beijing, China*

[b] *Collaborative Innovation Center on Forecast and Evaluation of Meteorological Disasters, NUIST, Nanjing, China*

ABSTRACT: Based on mosaics of composite radar reflectivity for a 4-year period from July 2007 to June 2011, a total of 354 mesoscale convective systems (MCSs) over central East China were identified and their characteristics were investigated. Using the objective classification method of obliquely rotated principal analysis in T mode, the atmospheric circulation patterns over central East China were classified into nine typical types based on the geopotential height fields at 850 hPa. It was found that 62.2% of daytime MCSs and 67.7% of nocturnal MCSs occurred in meridional atmospheric circulations, which were associated with the Western North Pacific Subtropical High (WNPSH) to the east and a low-pressure system to the west. The relationship between atmospheric circulation types and characteristics of MCSs was also investigated. Composite analyses revealed two different atmospheric circulation patterns at 500 hPa in meridional atmospheric circulations, the pre-short-trough pattern and the cold vortex pattern. The former featured relatively stronger vertical wind shear, warm advection, and convergence at the exit region of low-level jets (LLJs), while the latter was associated with relatively stronger frontal zones and frontogenesis process. Numbers of MCSs decreased significantly from 2008 to 2010, which might be attributed to changes in the location of WNPSH, the trough to the west and LLJs between the two systems.

KEY WORDS MCSs; central East China; objective classification; large-scale atmospheric circulation

Received 22 December 2015; Revised 12 September 2016; Accepted 19 September 2016

1. Introduction

Changes in extreme precipitation events are a major concern in both weather and climate research (Kunkel *et al.*, 1999; Zhai *et al.*, 2005). Climatic studies often focus on changes in total precipitation or extreme rainfall frequency and attribute them to the trends in sea surface temperature (SST), temperature of the atmosphere, strength of the monsoon systems, and other factors (Wang and Zhou, 2005; Goswami *et al.*, 2006; Panthou *et al.*, 2014). However, many studies have shown that mesoscale convective systems (MCSs) are responsible for a large portion of total rainfall amounts and many extreme rainfall events (Fritsch *et al.*, 1986; Schumacher and Johnson, 2005; Sun *et al.*, 2010). Schumacher and Johnson (2006) found that more than 70% of warm-season extreme rainfall events were caused by MCSs over the eastern two thirds of the United States. Exploring the connection between changes in MCS occurrence and large-scale atmospheric circulation provides another perspective on changes in extreme rainfall occurrence. Understanding MCS characteristics and their reliance on atmospheric circulation patterns could be the first step in understanding changes in extreme rainfall.

Early studies documenting the characteristics of MCSs around the world relied mostly on satellite data (Maddox, 1980; Velasco and Fritsch, 1987; Miller and Fritsch, 1991; Laing and Fritsch, 1993, 1997). In these studies, mesoscale convective complexes (MCCs), a particular category of MCSs with circular cloud shields, were documented, including their geographical distribution, durations, tracks, and diurnal and seasonal variations. Apart from tropical areas, a high frequency of MCCs was also observed in the Great Plains of the United States and in Southwest China, both in the mid-latitude region of the Northern Hemisphere (Laing and Fritsch, 1997). In China, although the frequency of MCCs was not as high as that observed in the United States Great Plains at the same latitude, more detailed surveys of MCSs, including elongated MCSs, revealed two regions of frequent MCS occurrence: central East China and Southwest China (Ma *et al.*, 1997; Zheng *et al.*, 2008a; Shu *et al.*, 2013). Recently, radar data became more widely used in MCS research (Bluestein and Jain, 1985; Geerts, 1998; Parker and Johnson, 2000) because radar is capable of distinguishing different convective patterns underlying similar cloud shields and has higher spatial and temporal resolution compared with satellite measurements (Jirak *et al.*, 2003). As radar echo is more closely connected to precipitation intensity in the reflectivity–rainfall rate (Z–R) relationship (Woodley *et al.*, 1975), it is more reasonable to identify MCSs using radar data when studying extreme precipitation. Many

* Correspondence to: Q. Zhang, Department of Atmospheric and Oceanic Sciences, School of Physics, Peking University, Beijing 100871, China. E-mail: qzhang@pku.edu.cn

studies investigated the organizational modes of MCSs using radar data and attempted to relate them to severe weather reports (Geerts, 1998; Parker and Johnson, 2000). In these studies, linear MCSs (i.e. squall lines) have received more attention due to their high frequency and high impact (Jirak *et al.*, 2003).

In China, fewer studies have used radar data due to the limited availability and quality of radar data. Meng *et al.* (2013) studied the general features of squall lines in eastern China and identified several high-frequency regions, including central East China and the southern coastal areas of China. Zheng *et al.* (2013) investigated the organizational modes of MCSs in summer during 2007–2010 over central East China and found that linear MCSs accounted for 55% of all MCSs. However, these studies only focused on linear MCSs (squall lines) or certain aspects of MCSs (e.g. organizational modes). It is apparent that both linear and non-linear MCSs produce torrential rains and flash flooding (Jirak *et al.*, 2003). Thus, a census of MCSs using radar data and employing criteria that incorporate various morphologies is still needed in China.

Both satellite and radar studies of MCSs have indicated that central East China is one of the most frequently affected areas by MCSs in China (Ma *et al.*, 1997; Zheng *et al.*, 2008a; Meng *et al.*, 2013; Shu *et al.*, 2013). The MCSs has caused numerous torrential rain and flash flooding events, resulting in many injuries and deaths across the region, as well as huge economic losses (Zheng *et al.*, 2013). Thus, this region is the main focus of our MCS study.

Synoptic-scale atmospheric circulation of MCSs has been examined both in China (Chen *et al.*, 1999; Zheng *et al.*, 1999; Sun *et al.*, 2005a) and in many other regions around the world (Maddox, 1983; Augustine and Caracena, 1994; Laing and Fritsch, 2000; Salio *et al.*, 2007). Most of these studies were based on case studies or composite analyses of a few cases. The typical features of synoptic-scale atmospheric circulation of a MCS include a weak mid-level short-wave trough, prominent baroclinic zones, a pronounced low-level jet (LLJ) coupled with strong lower-tropospheric warm advection, low-level convergence, and upper-level divergence related to upper-level diffluent flows. Subjective classification has also been used in the studies of convection environments (Tao, 1980; Sun *et al.*, 2005b; Meng *et al.*, 2013). Meng *et al.* (2013) subjectively categorized the atmospheric circulation patterns of squall lines over eastern China into six patterns, the most common of which was the pre-short-trough pattern.

However, most of the environmental factors and atmospheric circulation classifications discussed above were subjectively assessed; few objective atmospheric circulation classifications of the MCS environment were available. Although objective atmospheric circulation classification has been widely used in climatic research (Huth, 1993; Plaut and Simonnet, 2001; Kyselý and Huth, 2005), the attempt to apply such classification in MCS environments is still in its infancy. Using rotated principal component and cluster analysis, Peters and Schumacher (2014) found two subtypes of atmospheric fields associated with a large sample of heavy-rain-producing MCSs in the United States, the warm-season type and the synoptic type, which had distinct synoptic and mesoscale characteristics.

Additionally, previous summaries and atmospheric circulation classifications were based mostly on situations when MCSs occurred. It was a common for MCSs to have occurred in a synoptic pattern far from that considered favourable by the conceptual models used in previous works. Consequently, key or distinctive factors of a certain favourable synoptic pattern must be examined over a large sample size, based on a more general objective atmospheric circulation classification approach. This would provide a better understanding of the MCS environment, especially in central East China, where MCSs occur frequently.

The objectives of this study were to document the general features of MCSs and explore whether there was a connection between MCS occurrence and large-scale atmospheric circulation patterns over central East China. The remainder of the paper is organized as follows. Data and objective atmospheric circulation classification method are described in Section 2. Section 3 shows the spatial and temporal distributions of MCSs. The results of atmospheric circulation classification, as well as the relationship between atmospheric circulation types and characteristics of MCSs (e.g. intensity, duration, and track) are described in Section 4. A discussion and a summary are given in Sections 5 and 6, respectively.

2. Data and methodology

2.1. Composite radar reflectivity mosaics and definition of MCSs

The central East China, as shown in Figure 1, was defined as the region from 30° to 37°N, and 110° to 122°E, which was similar to the definition used by Zheng *et al.* (2013). The radar data used in this work were the digital mosaics of composite Doppler radar reflectivity, which were also used in Meng *et al.* (2013). Each pixel in the mosaics of composite radar reflectivity represented a real area of 4 km × 4 km. The time interval of the data was 20 (10) min before (after) 22 September 2008. The data started from July 2007, but more than 30% of the data were missing in 2012. Therefore, we chose records from July 2007 to June 2011 to ensure a relatively large and continuous data set. During this period, the average data coverage was about 85%, with the missing data randomly distributed in space and throughout each month.

Many definitions of MCSs have been proposed based on the different data used for their identification (Maddox, 1980; Parker and Johnson, 2000; Jirak *et al.*, 2003; Salio *et al.*, 2007). A widely accepted definition, given by the American Meteorology Society (AMS), was ‘a cloud system that occurs in connection with an ensemble of thunderstorms and produces a continuous precipitation area of the order of 100 km or more in horizontal scale

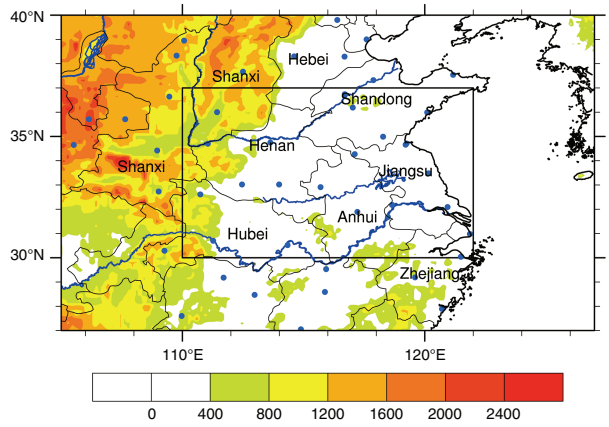

Figure 1. Terrain height (shading, units: m), related provinces and locations of radar stations over central East China. The light blue dots represent radar stations and the inner black box is central East China (30–37°N, 110–122° E). The shading indicates elevations higher than 400 m.

Table 1. Definitions of various radar traits of MCSs in this work.

Formation time	When the MCS definition is first met
Location of formation	Geometric centre of the MCS when it forms
Dissipation time	Time when the MCS definition was continuously last met for more than 3 h after its formation
Location of dissipation	Geometric centre of the MCS when it dissipates
Duration	Period during which the MCS definition is continuously met
Intensity	The maximum value of the radar composite reflectivity during its lifetime
First echo	The echo that first reaches the intensity of 40 dBZ tracked back from the formation of MCSs
Track	The lines which join the locations of the first echo, formation and dissipation of the MCS

in at least one direction' (Glickman and Zenk, 2000). Based on this definition, to incorporate MCSs of various morphologies, an MCS was defined as 'a continuous or quasi-continuous band of 40 dBZ reflectivity that extended for at least 100 km in at least one direction and lasted for at least 3 h' in this work, which was consistent with Parker and Johnson (2000) as well as Schumacher and Johnson (2006). The definitions of various radar traits of MCSs were given in Table 1. The MCSs were detected manually. Although it took a lot of work to identify MCSs case by case, the results may be considered more reliable compared with automatically detected MCSs.

2.2. Objective classification method

There are a wide variety of approaches and methodologies for classifying atmospheric circulation patterns, including the subjective, objective, and mixed methods (Huth and Coauthors, 2008). The method used in this study was obliquely rotated principal component analysis in T mode (T mode PCA) (Huth, 1996, 2000), and it could give more realistic and physically interpretable flow patterns compared to other objective atmospheric circulation classification methods (Compagnucci and Richman, 2008; Huth and Coauthors, 2008). Using the T mode PCA method, Zhao *et al.* (2013) studied the atmospheric circulation of the extreme torrential rain event that occurred on 21 July 2012 in Beijing, and quantitatively evaluated its extreme features. The method was made available in an open-source software called *cost733class*, which was developed in the COST Action 733 'Harmonization and Applications of Weather Type Classifications for European Regions'(Philipp *et al.*, 2014). The approach was briefly summarized below, and more details could be found in Huth (1996) and Huth (2000).

Compared with typically used principal component analysis (PCA), the T mode PCA method organized the data matrix so that grid point values were in rows and cases were in columns. After implementing PCA, a few leading principal components were retained and subjected to rotation to get more realistic and physically interpretable principal component patterns at the expense of losing maximum-variance and orthogonality property (Richman, 1986). Finally, each day was classified simply as the type (principal component) in which it has the highest loading (in the absolute sense).

The classification was based on the spatial distribution of geopotential heights at a particular level. Some previous studies implemented the classification based on geopotential height at 500 hPa (Huth, 1996) or sea-level pressure (Zhao *et al.*, 2013). In this study, after we implemented the classification based on geopotential height at different levels (500, 700, and 850 hPa) and sea-level pressure, we found that using geopotential height at 850 hPa, the classification could result in more realistic and physically interpretable flow regimes in this region.

The National Centers for Environmental Prediction (NCEP) Final (FNL) Operational Global Analysis data on $1° \times 1°$ grids at 6-h intervals (0000, 0600, 1200, and 1800 UTC) (see http://rda.ucar.edu/datasets/ds083.2/) were used for atmospheric circulation classification and analyses.

As the mechanisms of convection initiation may differ between the day and night, MCS days and nights were defined and studied, respectively. Considering the temporal availability of NCEP FNL data, a day was defined as being between 0000 UTC (0800 Beijing Time, Beijing Time = UTC + 8 h) and 1200 UTC (2000 Beijing Time), while a night was defined as being between 1200 UTC (2000 Beijing Time) and 0000 UTC (0800 Beijing Time) of the next day. Days (nights) on which at least one MCS occurred over central East China were defined as MCS days (nights). Days (nights) on which no MCS occurred over central East China were defined as Non-MCS days (nights). The data at 0000 UTC (1200 UTC) were used to investigate the atmospheric circulation during the day (night). In this way, we could focus on the atmospheric circulation before the formations of MCSs.

2.3. Composite analysis and significant test

After the classification of daily atmospheric circulation patterns, composite analyses were conducted to determine why MCSs occurred only on some days (nights) when the large-scale atmospheric circulation patterns were similar. The atmospheric circulations of MCS day (night) and Non-MCS day (night) for the same atmospheric circulation type were composited and compared. The composite analyses were only conducted in summer (June, July, and August) considering most MCSs occur in summer. Statistical test was implemented while comparing the atmospheric circulations of MCS day (night) and Non-MCS day (night). The significance of the difference of the means of some scalar variables between Non-MCS days (nights) and MCS days (nights) was estimated by *t*-test (Lau and Chan, 1983; Huang, 1989). The significance of the difference of the means of the winds was estimated by *F*-test (Shi *et al.*, 2004).

3. Spatial and temporal distributions of MCSs over central East China

With the definition in Section 2, a total of 354 MCSs (193 daytime MCSs and 161 nocturnal MCSs), 120 MCS days, and 107 MCS nights were identified from July 2007 to June 2011 over central East China, and some days (nights) were observed with multiple MCSs.

The spatial distributions of MCSs and their first echoes were shown in Figure 2(a) and (b), respectively. The largest frequency of MCS formation was near the boundaries of Anhui, Henan, and Shandong Provinces, which was consistent with the distribution of squall lines over this region in Meng *et al.* (2013). The region with largest frequency of first echoes of MCSs was about 1 degree west of the region with largest formation of MCSs. Another interesting fact was that most MCSs formed in lower elevation and relative flat terrain. Similar characteristics of squall lines and satellite-derived precipitation have been found by previous studies (He and Zhang, 2010; Meng *et al.*, 2013).

The diurnal and seasonal variation in MCSs over central East China was shown in Figure 3. About 76.6% (271 of 354) of MCSs occurred in summer (June, July, and August). Their diurnal variation showed postmeridian and nocturnal peaks with a significant peak after midnight in July. Apart from the diurnal and monthly variation in MCSs, another interesting fact was that the numbers of MCSs, MCS days, and MCS nights all decreased significantly from 2008 to 2010 (Figure 4, 2007 and 2011 were excluded from the statistics due to the availability of data). The decreased number of MCSs from 2008 to 2010 exceeded half of the total number in 2008 and was mainly contributed by MCSs in summer. The mechanism of the decline in the number of MCSs during the 3-year period was explored in Section 4.4.

The characteristics of MCSs over central East China displayed different characteristics in terms of their spatial and temporal variation. We further investigated other characteristics of MCSs in Section 4, including their tracks, intensity as well as duration, and their relationships with the atmospheric circulation patterns to determine if the variation could be explained from the atmospheric circulation patterns.

4. Atmospheric circulation patterns

In this section, we provided an objective classification of large-scale atmospheric circulation during the day and night over central East China. We analysed the MCS frequency, track, intensity, and duration for each atmospheric circulation type and searched for differences in the atmospheric circulation features between MCS day (night) and Non-MCS day (night) for the same atmospheric circulation type. Finally, we attempted to explain the decline in the frequency of occurrence of MCSs during the period 2008–2010.

4.1. Atmospheric circulation classification

The T mode PCA method was more frequently used in long-term climate analyses (Huth, 2000; Kyselý and Huth, 2005), whereas the time period of interest in our study was relatively short. What's more, numbers of MCSs decreased significantly from 2008 to 2010, as indicated in Section 3. To eliminate the influence of interannual variation, a classification was implemented with a 12-year data sample covering the time period of interest (from 1 July 2001, to 30 June 2013, a total of 12 years), and then the atmospheric circulation types in the time period of interests were identified within the classification. The spatial patterns of geopotential height at 850 hPa (from 15° to 50° N and 100° to 135° E) were classified into nine types using T mode PCA. The number of types (principal components retained and rotated) was determined according to the variance explained by the principal components (Table 2) and their physical interpretability of the classified atmospheric circulation patterns. Multiple tests were implemented before the final decision was made. After rotation, the differences of the variance explained by different principal components became relatively small, so the classification may not be dominated by one or two types that explained most of the total variance.

The results of classification for daytime atmospheric circulation were shown in Figure 5(a). The nine daytime atmospheric circulation types were termed daytime types (DT) 1–9. The monthly frequency distribution of atmospheric circulation types was given in Figure 6(a). It was shown that for different atmospheric circulation types, different weather systems influenced central East China (Figure 5(a), also observed in composite sea-level pressure fields, which are not shown). In DTs 1 and 2, strong high-pressure systems dominated northern China in sea-level pressure fields (not shown), and there was a slight difference in the location of the high-pressure systems between the two types. DTs 3 and 5 were meridional atmospheric circulation types, with central East China on the west edge of the Western North Pacific Subtropical

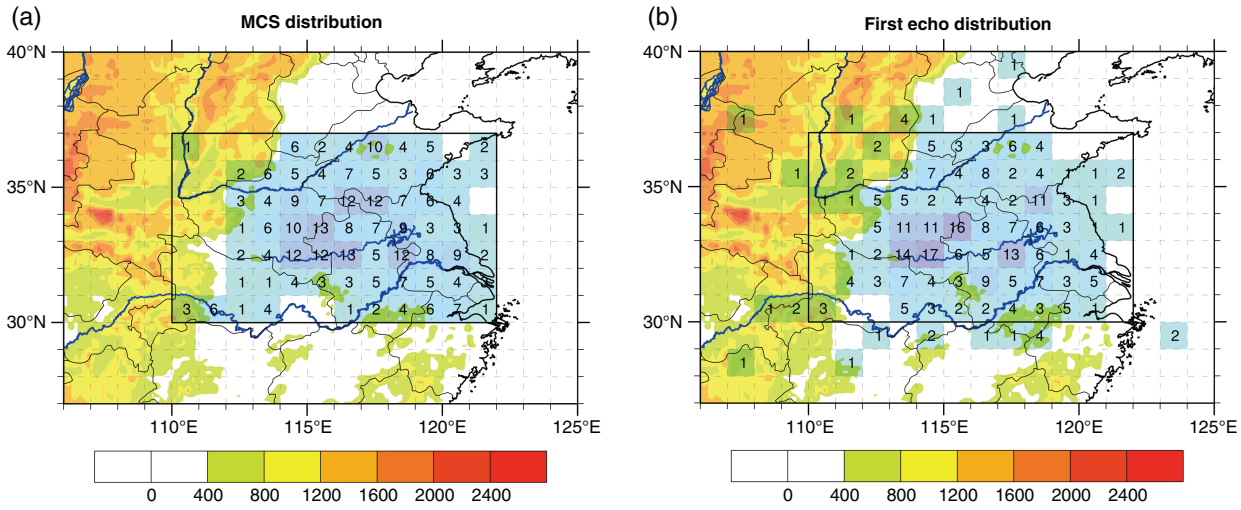

Figure 2. Spatial distribution of MCSs (a) and their first echoes (b) over central East China from July 2007 to June 2011. Each number in the box represents the number of MCSs (first echoes) in a 1° × 1° box. The inner black boxes are central East China (30–37°N, 110–122° E). The shading indicates elevations (units: m) higher than 400 m as in Figure 1.

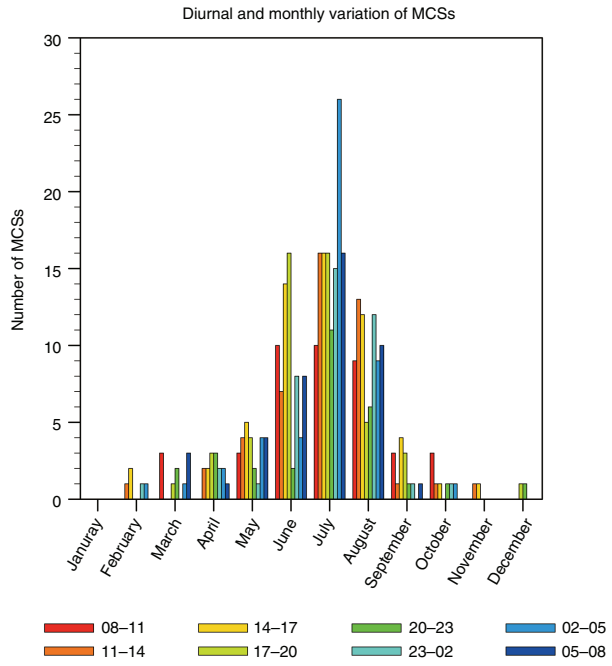

Figure 3. Seasonal and diurnal variation in MCSs over central East China from July 2007 to June 2011. Bars of different colours represent the hour of newly formed MCSs observed in 3-h intervals. Time used here is Beijing Time.

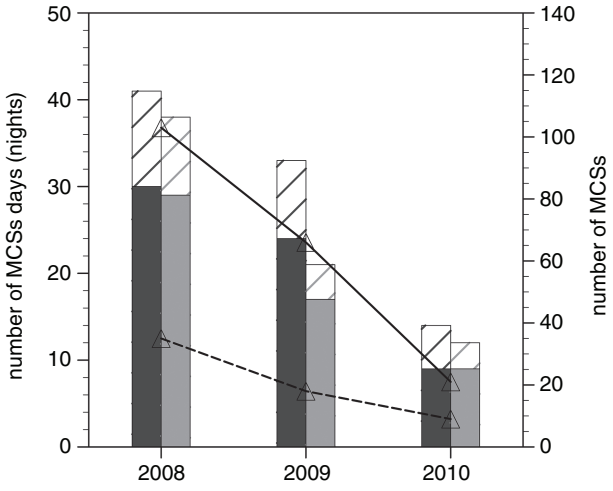

Figure 4. Variation in numbers of MCS and MCS days (nights) over the Central East China from 2008 to 2010. The dark grey (light grey) bars represent the numbers of MCS days (nights) and their tick marks are marked on the left y axis. The solid (hatched) part of the bars represents the numbers of MCS days or nights in summer (other seasons). The solid (dashed) line represents the number of MCSs in summer (other seasons) and their tick marks are marked on the right y axis. The number of MCSs in each year is marked by a triangle.

High (WNPSH) and a low pressure to the west at 850 hPa (Figure 5(a)). There were differences between the two DTs. The WNPSH in DT 3 extended more westward with a trough to the west, whereas DT 5 featured a strong low-pressure system at 850 hPa over northern China. In DTs 6 and 7, a ridge or high-pressure system dominated central East China. In DTs 8 and 9, central East China was under the influence of the atmospheric circulation induced by a tropical cyclone over the ocean.

The seasonal variation in frequency of atmospheric circulation types was consistent with the seasonal variation in different weather systems (Figure 6(a)): DTs 1 and 2 mainly occurred in winter, which were possibly related to the active cold air, whereas DTs 3 and 5 occurred mainly in summer. The atmospheric circulation types with tropical cyclones (DTs 8 and 9) had peaks in summer and autumn, which was consistent with the seasonal distribution of tropical cyclones in the Western North Pacific (Sun *et al.*, 2011).

By comparing the occurrence frequency (defined as the number of MCS days for a particular atmospheric circulation type divided by the total number of days belong to that atmospheric circulation type: see the percentages in the top right of each panel in Figure 5(a)) of MCSs, it

Table 2. Percentage of variance explained by each unrotated and rotated principal components (Unit:%) during the day and night. For each term, the left column shows the variance explained by the n-th principal component, and the right column shows the accumulated variance explained by the leading n principal components.

Principal component	Unrotated (day)		Unrotated (night)		Rotated(day)		Rotated(night)	
1	47.70	47.70	44.35	44.35	10.99	10.99	10.70	10.70
2	14.64	62.34	17.14	61.49	9.00	19.99	9.18	19.88
3	8.48	70.82	8.46	69.95	8.94	28.93	9.17	29.04
4	6.67	77.48	7.32	77.27	8.53	37.46	9.16	38.20
5	5.00	82.48	4.63	81.90	7.80	45.26	8.26	46.46
6	2.73	85.21	3.07	84.98	7.34	52.60	7.75	54.21
7	2.22	87.44	2.33	87.31	7.11	59.71	7.51	61.72
8	1.78	89.22	1.78	89.09	6.91	66.63	7.18	68.90
9	1.30	90.51	1.31	90.41	6.65	73.28	6.17	75.06

could be seen that the occurrence frequency of MCSs in meridional atmospheric circulation types (DTs 3 and 5) was significantly higher (16.3% and 21.0%, respectively) than for the other atmospheric circulation types (no more than 10%). Although meridional type days accounted for 28.2% of all days (412 of 1461 days), 62.2% of daytime MCSs (120 of 193) and 60.8% of MCS days (73 of 120) occurred in these two atmospheric circulation types. Meridional atmospheric circulation types were favourable for the transportation of water vapour from the South China Sea, and the active trough to the west also played an important role in convection environment, which was similar to the meridional types found in the subjective classification of Tao (1980).

The atmospheric circulation patterns at night shown in Figure 5(b) were similar to the daytime atmospheric circulation. As the patterns of explained variance during the day and night were similar (Table 2), the nocturnal atmospheric circulation was classified into nine types to be consistent with daytime atmospheric circulation. The nine nocturnal atmospheric circulation types were referred to as nocturnal types (NTs) 1–9. Strong high-pressure systems dominated northern China in NTs 1, 3, and 4, with slight difference of location and intensity of the high-pressure systems (Figure 5(b), more evident in composite sea-level pressure field, not shown). NTs 2 and 7 were also meridional types having typical features in common with daytime meridional types, including the position of the WNPSH and low-pressure systems to the west. NTs 5 and 8 had ridges extending to central East China. Similar to DTs 8 and 9, NTs 6 and 9 were under the influence of atmospheric circulation induced by tropical cyclones over the ocean. Just as daytime atmospheric circulation types, seasonal variation in frequency of atmospheric circulation types corresponded well with the seasonal variation in weather systems (Figure 6(b)). The highest frequency of MCS occurrence was also observed in meridional atmospheric circulation types (NTs 2 and 7). Although NTs 2 and 7 accounted for 30.5% of all nights (446 of 1461 nights), 67.7% of nocturnal MCSs (109 of 161) and 61.7% of all MCS nights (66 of 107) occurred in these two atmospheric circulation types. Owing to the high occurrence frequency of MCSs in the meridional atmospheric circulation types, the atmospheric circulations of these types were further investigated using a composite analysis method, as discussed in Section 4.3.

4.2. Relationships between atmospheric circulation types and the characteristics of MCSs

The relationships between atmospheric circulation types and MCS intensities, durations, and tracks were also investigated, and some MCSs with missing values (16, 10, 5, and 11 cases with missing first echo, dissipation, intensity, and duration data, respectively) were simply excluded in the study. As shown in Figure 7(a), the tracks of daytime MCSs were largely determined by the atmospheric circulation type. The MCSs in DTs 1 and 2 tended to move towards the east or southeast, probably dominated by the background northwestern or western steering winds in the mid troposphere in winter. MCSs in meridional atmospheric circulation types had tracks mostly towards the east and southeast, and a few towards northeast, while MCSs in DT 9, which was associated with tropical cyclones, mainly moved northward. Comparing the durations of MCSs in the different atmospheric circulation types, it was found that MCSs in the meridional atmospheric circulation types had a longer duration than in other atmospheric circulation types, with 80.0% of the MCSs having durations longer than 9 h (24 of 30) being distributed in these types. Few MCSs were observed with duration longer than 9 h in the cold front types (DTs 1 and 2). The MCSs in DT 9 which was associated with tropical cyclones also had short durations. The distribution of daytime MCS intensities in different atmospheric circulation types was shown in Figure 8(a). The distributions of MCS intensities were very similar to those of the MCS durations, which meant that long-lasting MCSs tended to have stronger intensities than short-term ones.

From Figures 7(b) and 8(b), it was shown that the distribution patterns of the intensities, durations, and tracks of nocturnal MCSs were similar to those of daytime MCSs. However, few MCSs were observed in atmospheric circulation types associated with tropical cyclones (NTs 6 and 9) at night. Nocturnal MCS intensities were relatively weak compared to daytime MCSs (Figure 8(b)), with daytime intensities peaking at 60–65 dBZ and nocturnal

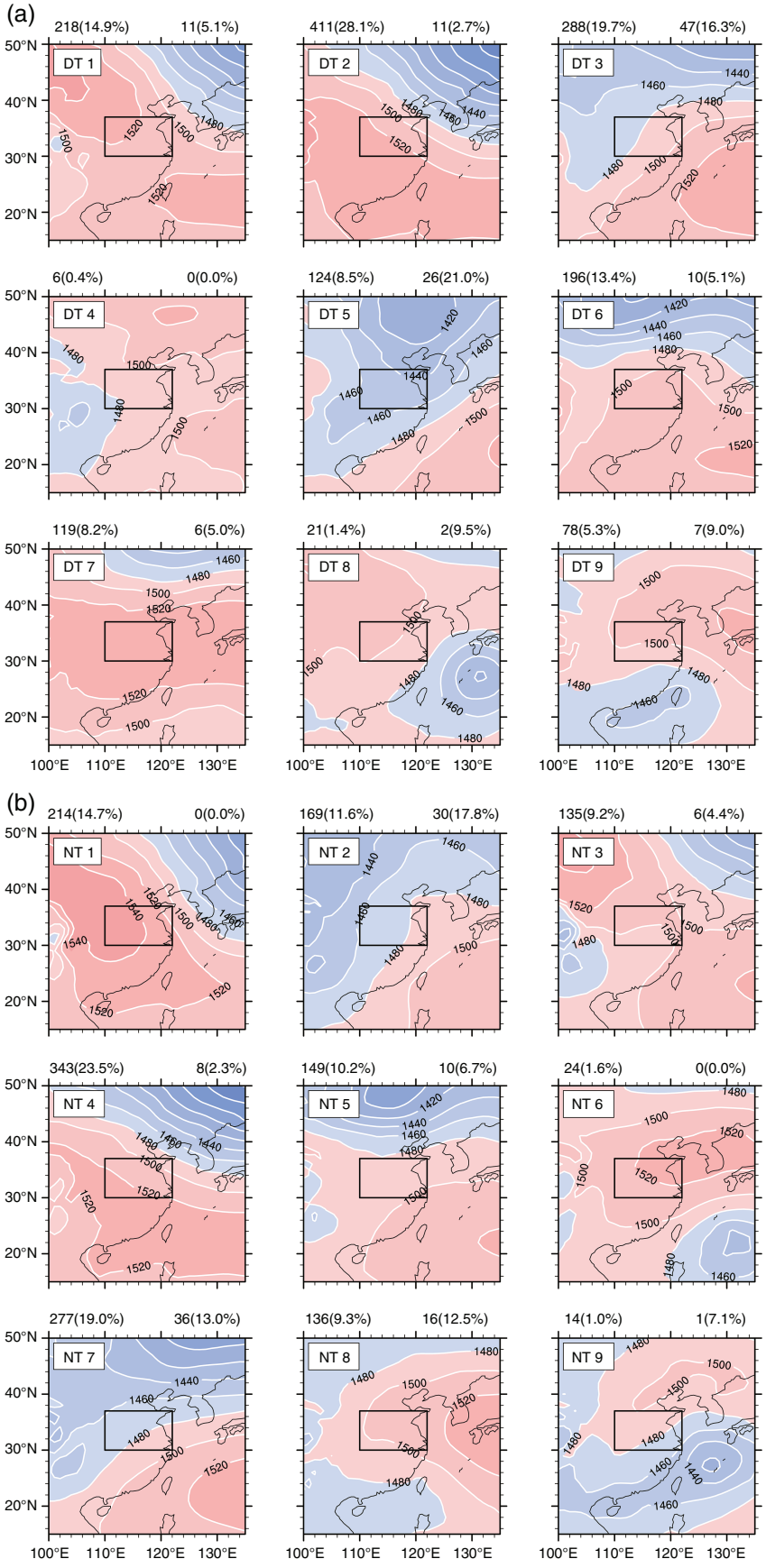

Figure 5. The nine daytime circulation types [daytime types (DTs) 1–9, figure (a)] and nine nocturnal circulation types [nocturnal types (NTs) 1–9, figure (b)) based on geopotential height at 850 hPa (units: gpm) over central East China from July 2007 to June 2011. The number of days for each circulation type and their percentages are shown in the top left; the number of MCS days and the frequency of MCS occurrence for each circulation type are shown in the top right of each panel. The inner black boxes in each panel are central East China (30–37°N, 110–122°E).

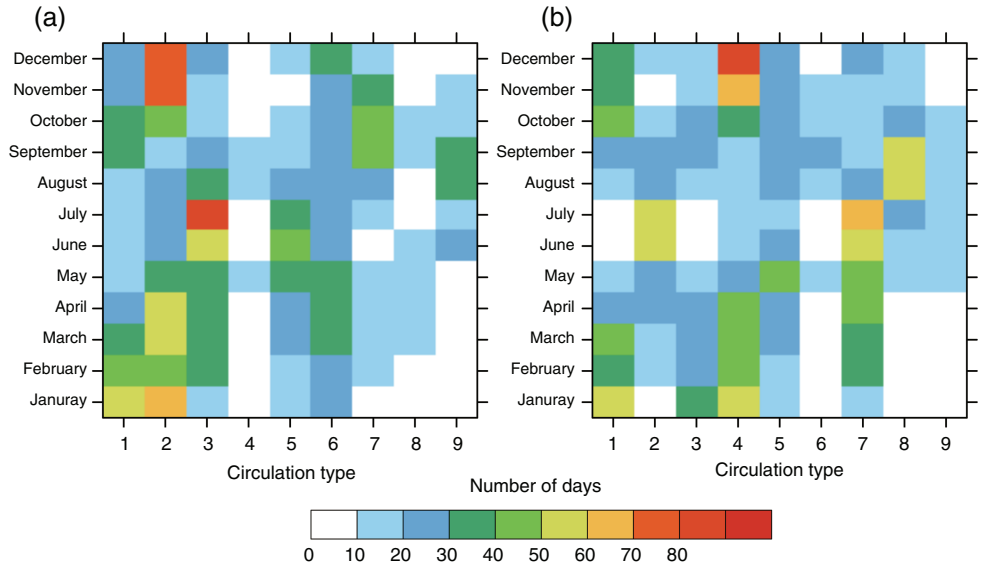

Figure 6. Monthly variations in number of days (a) and nights (b) for each circulation type over central East China from July 2007 to June 2011. Each box with different colour represents the number of days (nights) in the corresponding circulation type and month.

intensities peaking at 55–60 dBZ. This indicated that solar heating might play an important role in the development of MCSs.

4.3. Composite analyses of meridional atmospheric circulation types

The results of composite analyses for Non-MCS and MCS days (nights) were shown in Figures 9 and 10. In DT 3, central East China was on the west edge of the WNPSH with a weak trough to the west at 500 hPa (Figure 9(a) and (b)), and therefore this pattern was termed the pre-short-trough pattern for simplicity. Significant difference exceeding the 95% confidential limits in the geopotential height fields (dotted areas in Figure 9(a) and (b)) was the northwestward extending of WNPSH and the deeper trough (the trough is near 39°N 112°E in Figure 9(a) and (b)) on MCS day compared with Non-MCS day. The stronger WNPSH and deeper trough on MCS days were associated with a sharper pressure gradient than Non-MCS days over the southeast of China, which was favourable for the strengthening of southwesterly LLJs over the southeast of China (vectors in Figure 9(a) and (b), plotted were winds whose difference between Non-MCS and MCS days exceeded the 95% confidential limits). The LLJs played important roles in the convection environment: (1) LLJs continuously transported unstable warm moist air [indicated by equivalent potential temperature and Best Lifted Index (BLI) (WMO, 1992) in Figure 10(a) and (b)] from southeast China to feed the convection; (2) veering of the winds from southwesterly winds at 850 hPa to westerly winds at 500 hPa enhanced the vertical wind shear over central East China (shadings in Figure 9(a) and (b)); (3) warm advection indicated by the veering of the winds and convergence at the exit region of the LLJs provided the forcing of lift.

However, compared with DT 3, the atmospheric circulation patterns of DT 5 were totally different. The Northern China was dominated by a cold vortex, with a much weaker WNPSH in DT 5 (Figure 9(c) and (d)), and this pattern is therefore termed the cold vortex pattern for simplicity. No pronounced LLJs were observed over southern China, and cold air intruded from the northeast, which was associated with the stronger cold vortex over northern China on MCS days than Non-MCS days. Convergence of northerly and southerly flow was associated with much stronger frontal zones and frontogenesis process in DT 5 compared with DT 3 (Figure 10(b) and (d)), which provided important forcing for convection in the cold vortex pattern. The frontogenesis process was indicated by the 2D frontogenesis function (Miller, 1948; Martin, 1998) in Figure 10:

$$F_{2D} = \frac{1}{|\nabla\theta|}\left[-\frac{\partial\theta}{\partial x}\left(\frac{\partial u}{\partial x}\frac{\partial\theta}{\partial x}+\frac{\partial v}{\partial x}\frac{\partial\theta}{\partial y}\right) -\frac{\partial\theta}{\partial y}\left(\frac{\partial u}{\partial y}\frac{\partial\theta}{\partial x}+\frac{\partial v}{\partial y}\frac{\partial\theta}{\partial y}\right)\right]. \quad (1)$$

Considering the Meiyu Front was frequently defined as narrow zones where equivalent potential temperature gradient maximized (Zheng *et al.*, 2008b), the potential temperature in Equation (1) was replaced by equivalent potential temperature.

In brief, the large-scale atmospheric circulation patterns differed between these two meridional daytime atmospheric circulation types. DT 3 (pre-short-trough pattern) featured strong vertical wind shear as well as convergence and warm advection at the exit region of the LLJs, whereas DT 5 (cold vortex pattern) had stronger frontal zones and frontogenesis process than DT 3. The typical features of DT 3 and the important role of LLJs were similar to the previous studies mentioned in Section 1. Features of DT 5 were less documented in previous studies, which might be associated with the relative less numbers of MCS Days compared with DT 3.

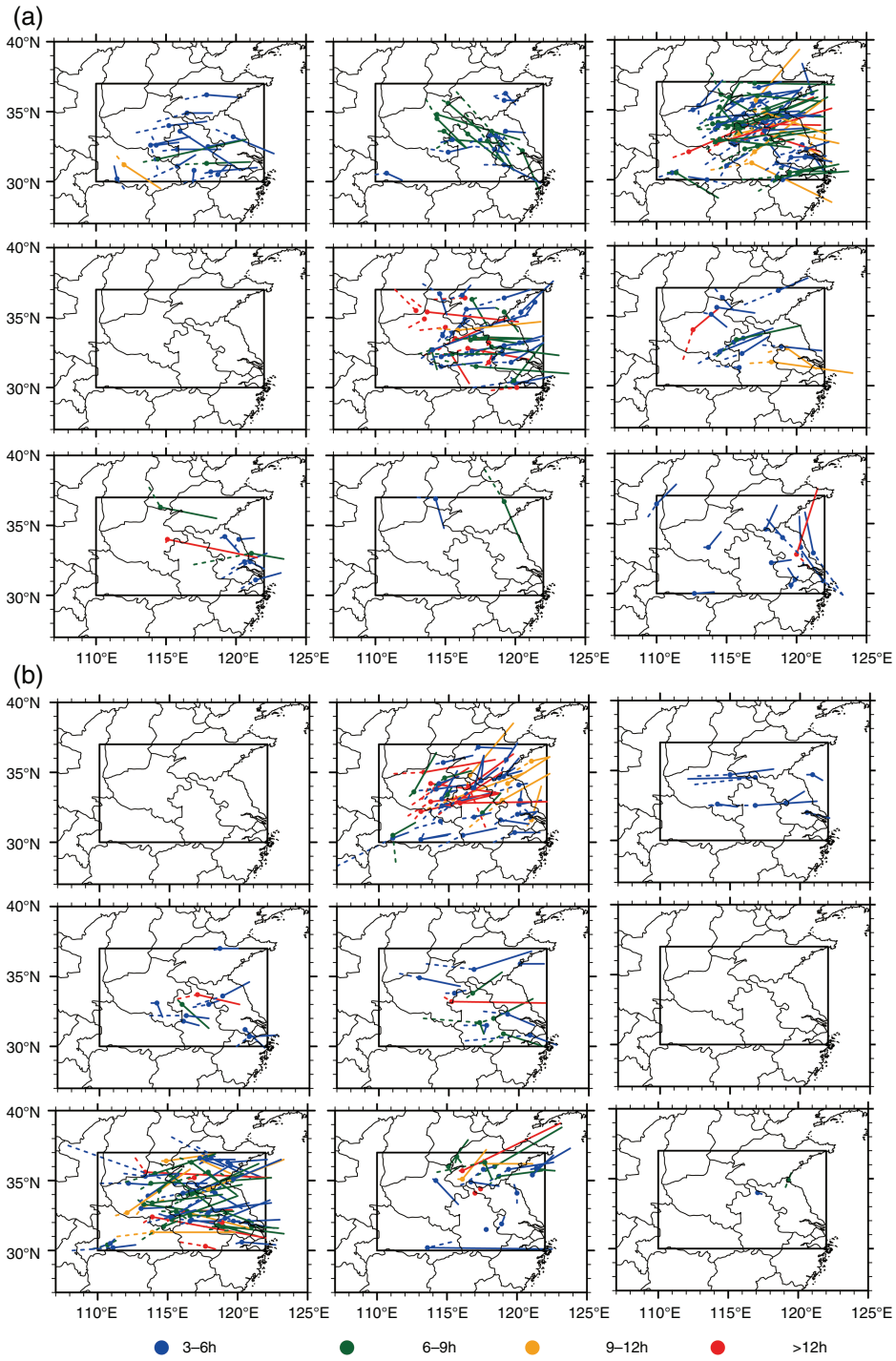

Figure 7. MCS tracks corresponding to each daytime circulation type (a) and nocturnal circulation type (b) in Figure 5. Different colours represent MCSs of different duration. The location of each MCS formation is represented by a dot. The dashed line is the track from the first echo to MCS formation and the solid line is the track from MCS formation to dissipation. Corresponding parts of tracks of MCS with missing first echo or dissipation locations were not drawn here. The inner black boxes in each panel are central East China (30–37°N, 110–122°E).

A comparison of nocturnal composite atmospheric circulations (Figure 9(e)–(h)) revealed that the main differences between MCS and Non-MCS nights were the intensity and forcing of LLJs. In NT 2 (Figure 9(e) and (f)), although the LLJs and their associated forcing were relatively weak due to the northward shifting of WNPSH, rather than westward extending, basic features of this type were very similar to those of pre-short-trough pattern (DT 3), including the WNPSH, the trough to the west, and the LLJs between them. In NT 7 (Figure 9(g) and (h)), the LLJs and their associated forcing were very strong, and this also resembled the features of pre-short pattern. So the nocturnal atmospheric circulation patterns were more similar to the pre-short-trough pattern than the cold vortex pattern in daytime. Typical features of the cold vortex pattern (DT 5), including the intrusion of cold air, strong

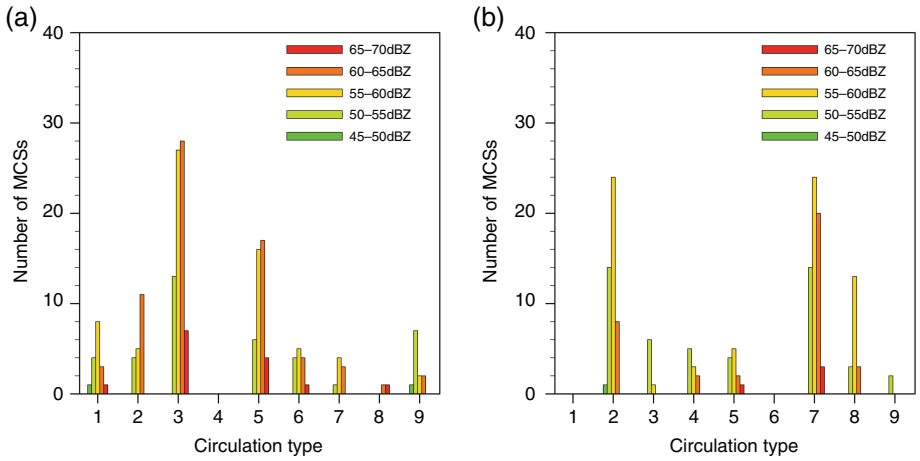

Figure 8. MCS intensities of different daytime (a) and nocturnal (b) circulation types over central East China from July 2007 to June 2011.

frontal zones, and frontogenesis process, were not obvious at night. This result was consistent with the diurnal variation of convection which peaks in the afternoon in the cold vortex flow regime (Yu *et al.*, 2011). Therefore, it may be inferred that solar heating may play an important role in the convection environment of cold vortex patterns (DT 5). In contrast, the stronger intensity of LLJs on MCS nights compared to Non-MCS nights (Figure 9(e)–(h)) suggested a more important role of the forcing of LLJs. The importance of nocturnal LLJs was consistent with the results of several other studies that have established the connection between the nocturnal LLJ maximum and tendency for nocturnal rainfall in China (Chen *et al.*, 2009; Liu *et al.*, 2012; Chen *et al.*, 2013; Wang *et al.*, 2013).

4.4. Possible mechanism of the decline in the numbers of MCSs from 2008 to 2010

To explain the decline in the number of MCSs from 2008 to 2010 shown in Figure 4, the variation in atmospheric circulation types over the 3-year period was also investigated. According to Figure 11, the number and probability of MCS days and nights mainly decreased in meridional types (DTs 3 and 5, NTs 2 and 7) from 2008 to 2010. Owing to the similarities of atmospheric circulation patterns and environmental conditions between DT 3 and nocturnal meridional types (NTs 2 and 7) which has been discussed in Section 4.3, we conducted analyses on the three types together, which contributes most to the number and decline in MCS occurrence (Figure 11). In contrast, the number of days in DT 5 decreased significantly from 2008 to 2009, which may partly account for the decreasing of MCS days in DT5 from 2008 to 2009.

Figure 12 showed the changes in composite fields of DT 3, NTs 2 and 7 over central East China from 2008 to 2010. Just as in the composite study, the composite analyses were conducted only in summer. To determine their variation during the 3 years, we calculated the mean wind fields at 850 hPa for the summer of the 3 years, and then the mean wind fields were subtracted from wind fields of each year to get their anomaly wind fields respectively for each year (Figure 12). The variation in the WNPSH (defined as areas where geopotential heights were greater than 5880 gpm) and the trough to the west were the most noticeable and distinct features in the 500 hPa geopotential height fields during the 3-year period.

In 2008, the weak WNPSH and significant trough over south China induced a cyclonically curved atmospheric circulation (A in Figure 12(a)) downstream of the trough in the anomaly wind fields. This cyclone atmospheric circulation helped to strengthen the LLJs over southeastern China (corresponding to the location of the LLJs in Figure 9(a) and (b), and (e)–(h)), and the cyclonically curved atmospheric circulation anomaly that extended to central East China also enhanced convergence over this region. In 2009, the absence of the trough over south China induced an anticyclonically curved atmospheric circulation (B in Figure 12(b)) in the anomaly wind fields over central East China, which was unfavourable for both water vapour transportation and convergence compared to the situation in 2008. In 2010, the southward shift of the WNPSH induced a cyclone atmospheric circulation anomaly over the East China Sea (C in Figure 12(c)). Atmospheric circulation anomaly C decreased water transportation from the south to the target area when superimposed on background southwesterly winds, which may have inhibited convection compared to the previous 2 years.

In conclusion, the decline in MCS occurrence in central East China can be attributed to changes in the large-scale atmospheric circulation including the WNPSH, the trough over south China, and the LLJs between the two systems and the variation in strength of LLJs may be a key factor.

5. Discussion

The importance of meridional atmospheric circulation for convection has been noticed by many researches in eastern China (Tao, 1980; Zhao *et al.*, 2013), and our findings that most MCSs occurred in meridional types were consistent with previous results. But even in meridional atmospheric circulation types, the frequency of MCSs was no more than 25% (Section 4.1 and Figure 5). Using the method of

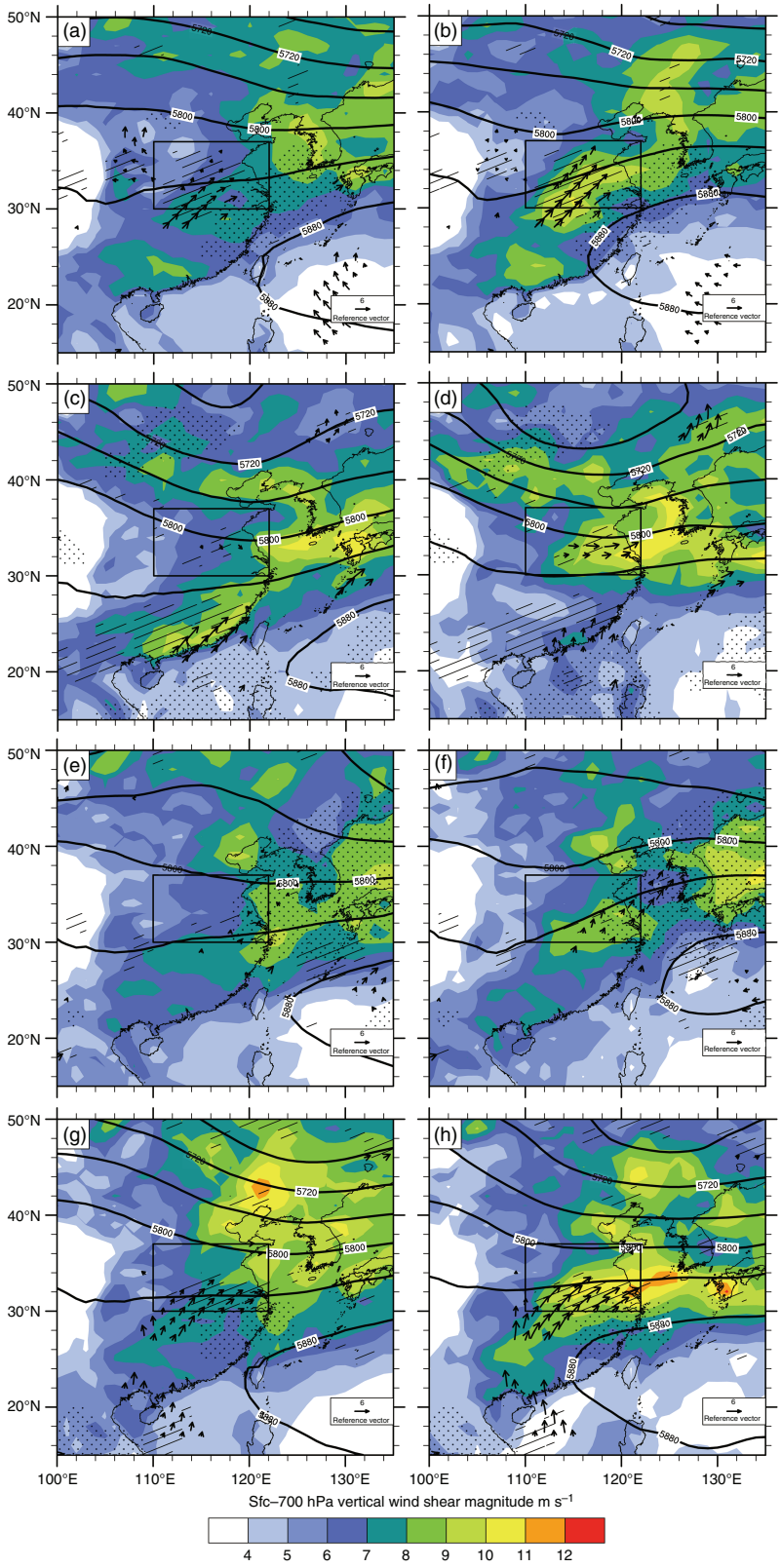

Figure 9. Composite analyses for Non-MCS days of DT 3 (a), MCS days of DT 3 (b), Non-MCS days of DT 5 (c) and MCS days of DT 5 (d) Non-MCS days of NT 2 (e), MCS days of NT 2 (f), Non-MCS days of NT 7 (g) and MCS days of NT 7 (h) over central East China from July 2007 to June 2011. The plot shows geopotential height at 500 hPa (black contours, units: gpm, at intervals of 40 gpm, areas where the difference of the means between MCS and Non-MCS days exceeds the 95% confidence limits, are dotted), vertical wind shear magnitude between surface and 700 hPa (shadings, units: m s^{-1}, areas where the difference of the means between MCS and Non-MCS days exceeds the 95% confidence limits are hatched), winds at 850 hPa (black vectors, units: m s^{-1}; winds are only plotted where the difference of the means between MCS and Non-MCS days exceeds the 95% confidence limits). The inner black boxes in each panel are central East China (30–37°N, 110–122°E).

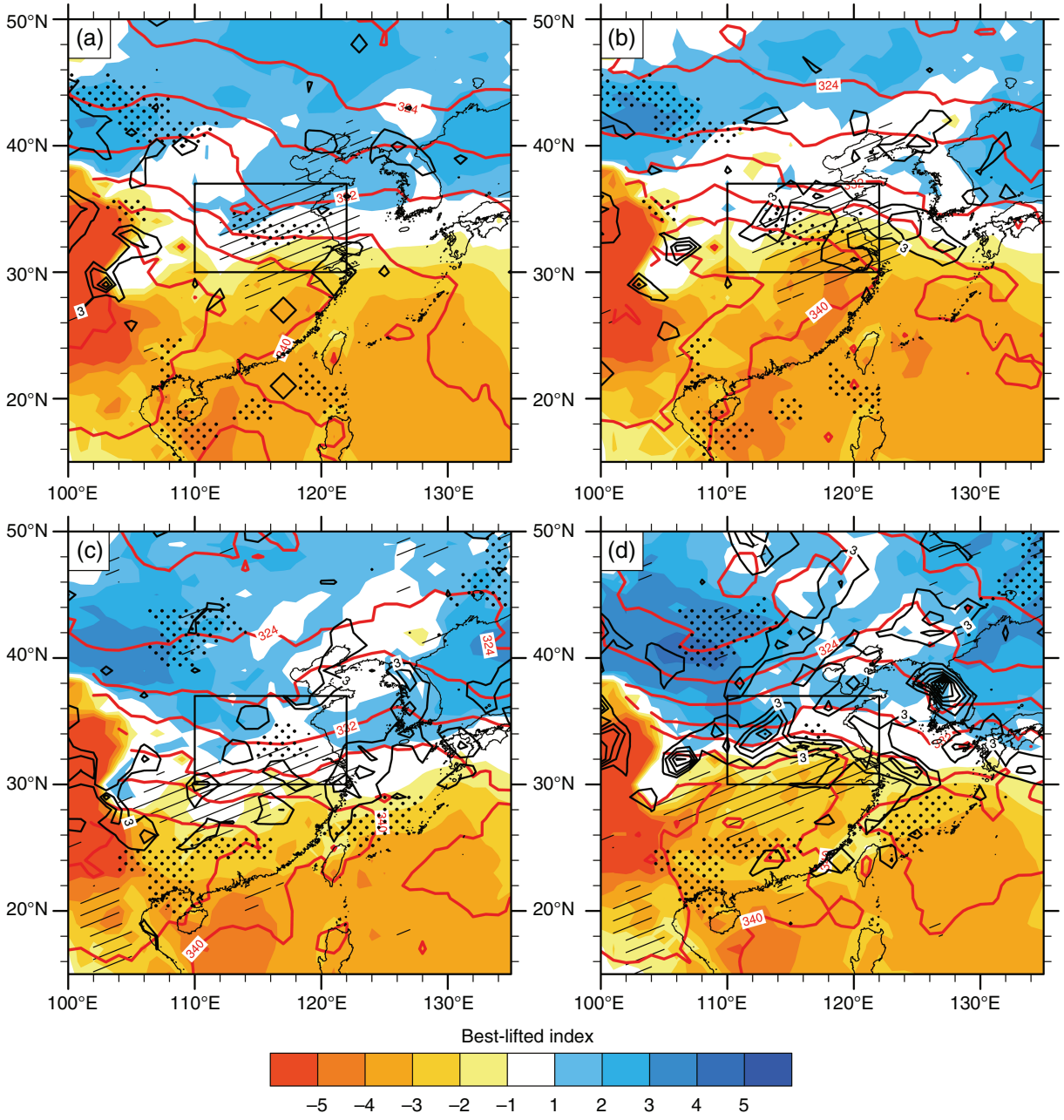

Figure 10. Composite analyses for Non-MCS days of DT 3 (a), MCS days of DT 3 (b), Non-MCS days of DT 5 (c) and MCS days of DT 5 (d) over central East China from July 2007 to June 2011. The plot shows Best Lifted Index (BLI) (shadings, units: K, areas where the difference of the means between MCS and Non-MCS days exceeds the 95% confidence limits are hatched), equivalent potential temperature at 700 hPa (red solid contours, units: K, at intervals of 4 K, contours where elevations are higher than 700 hPa have been removed, areas where the difference of the means between MCS and Non-MCS days exceeds the 95% confidence limits are dotted) , horizontal frontogenesis (black lines, units: 10^{-10} K s^{-1}, at intervals of 2×10^{-10} K s^{-1}, contours with values less than 3×10^{-10} K s^{-1} have been removed). The inner black boxes in each panel are central East China (30–37°N, 110–122°E).

composite analyses, this study found key factors of MCS environments in meridional types, which were the forcings of LLJs. The important role of LLJs in MCS environments was also found in other monsoon regions around the world as well (Augustine and Caracena, 1994; Laing and Fritsch, 2000; Salio *et al.*, 2007).

Previous researches have shown that compared with unorganized convection, environments of MCSs often had stronger large-scale forcing (Raymond and Jiang, 1990; Lewis and Gray, 2010; Markowski and Richardson, 2010; Wang *et al.*, 2014). Our results agreed well with these findings. Large-scale atmospheric circulation patterns not only controlled the activity of MCSs in intraseasonal scale (Augustine and Howard, 1991; Zheng *et al.*, 1999), but also dominated the interannual variation in MCS numbers (Section 4.4). However, due to the availability of radar data, the 4-year period was relatively short in climate sense, but this work may provide a new view and methodology to study the change of extreme precipitation. Future work may include cross validation of radar

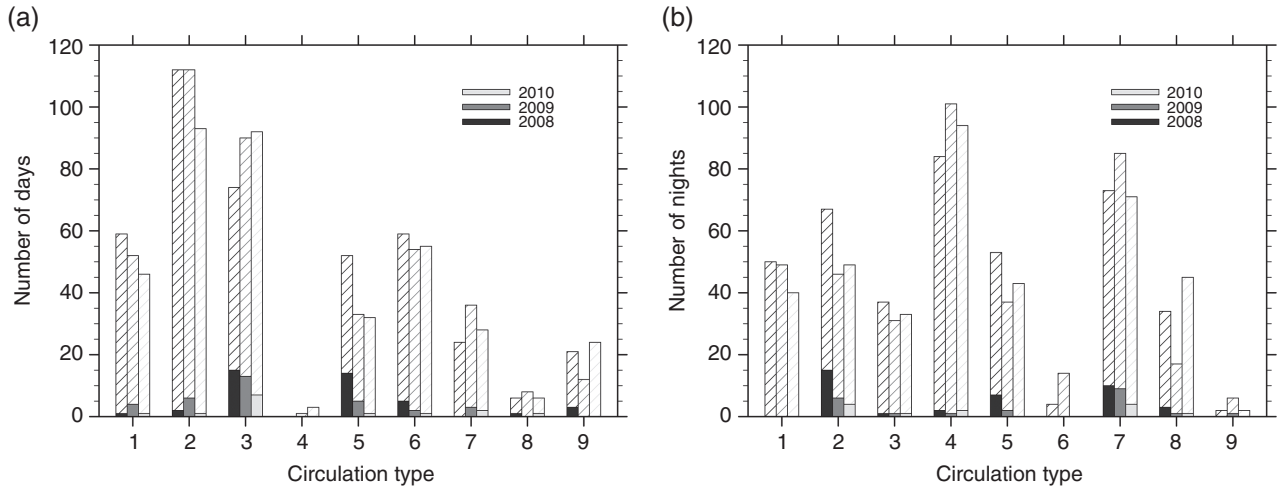

Figure 11. Variation in daytime circulation types and MCS day types (a), nocturnal circulation types and MCS night types (b) over central East China from 2008 to June 2010. Hatched bars are Non-MCS days, filled bars are MCS days.

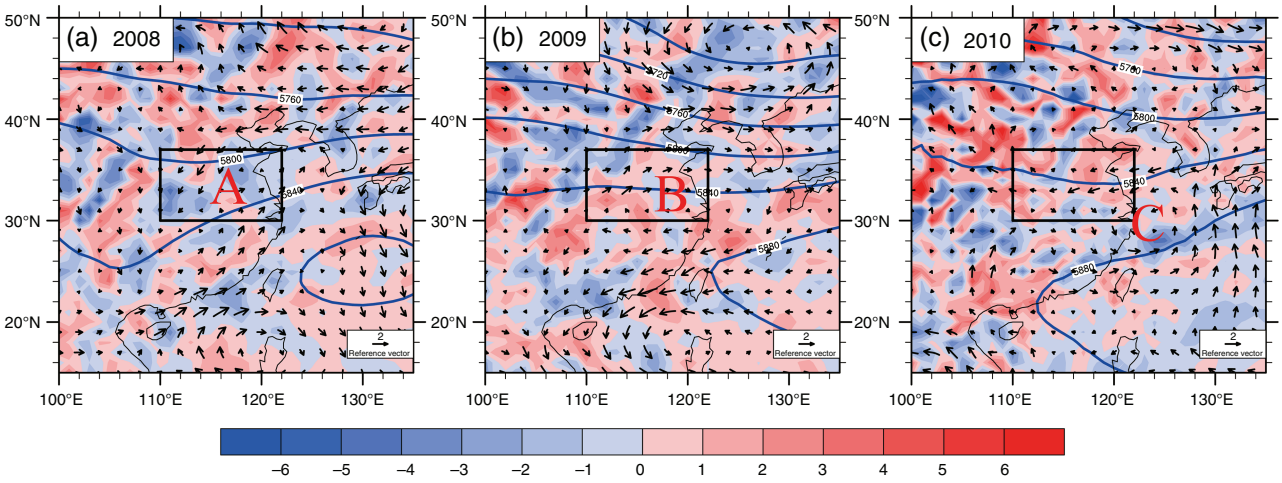

Figure 12. Changes in composite circulations of DT 3, NTs 2 and 7 over central East China in summer from 2008 to 2010. The plot shows geopotential height at 500 hPa (thick blue contours, units: gpm, at intervals of 40 gpm), wind anomalies (black vectors, units: m s^{-1}), divergence of wind anomalies (shadings, units: 10^{-6} s^{-1}). The bold red letters A–C in each panel mark the centres of anomaly circulations indicated by wind anomalies. The inner black boxes in each panel are central East China (30–37°N, 110–122°E).

and satellite or precipitation data which has much better data coverage, based on which the identification of MCSs and the connection between MCSs and large-scale atmospheric circulation patterns could be extended to a much longer period, and better understanding of the long-term variation of extreme precipitation could be gained in this process. As pointed out by Huth (2000), the daily classification method could be applicable to climate models. With the connection between MCSs and large atmospheric circulation, the climate model may provide us information about the trend of extreme rainfall in the future.

This study mainly focused on large-scale environments of MCSs. Although large-scale atmospheric circulations dominate the MCS occurrence, the onset time and location of MCSs cannot be determined by large-scale atmospheric circulation, so further studies of mesoscale environment features are also needed. The central East China are frequently affected by mesoscale vortices, including the Dabie Vortices (Fu *et al.*, 2016), the Tibetan Plateau Vortices (Feng *et al.*, 2014), and the southwest vortices (Wang and Tan, 2014). Mesoscale vortices are found to be important triggers of MCSs, and MCSs would, in turn, generate new vortices and intensify pre-existing vortices (Bartels and Maddox, 1991; Davis and Trier, 2002; Houze, 2004; Schumacher and Johnson, 2008; Sun *et al.*, 2010). Further studies of the interaction between mesoscale vortices and MCSs would help to better understand the formation mechanisms of MCSs.

6. Conclusion

Based on mosaics of composite radar reflectivity radar data over a 4-year period from July 2007 to June 2011, this study documented the general features of MCSs over central East China and investigated the connection between the occurrence of MCSs and large-scale atmospheric

circulation. The main conclusions of this work are summarized as follows:

- About 76.6% of MCSs occurred in summer which is June, July, and August. The diurnal variation of MCSs showed postmeridian and nocturnal peaks with a significant peak after midnight in July. The highest frequency of formation was near the boundaries of Anhui, Henan, and Shandong Provinces. Both the frequency of MCSs and MCS days (nights) decreased pronouncedly from 2008 to 2010.
- Using the objective classification method of T mode PCA, atmospheric circulations over central East China were classified into nine typical types based on the geopotential height fields at 850 hPa, of which 62.2% of daytime MCSs and 67.7% of nocturnal MCSs occurred in meridional atmospheric circulation types.
- The composite analyses revealed two different atmospheric circulation patterns at 500 hPa in daytime meridional atmospheric circulation types, the pre-short-trough pattern and the cold vortex pattern. The former featured relatively stronger vertical wind shear, warm advection, and convergence at the exit region of LLJs, while the latter vortex pattern featured stronger frontal zones and frontogenesis process.
- The decline in frequency of MCSs in central East China from 2008 to 2010 can be attributed to changes in large-scale atmospheric circulation patterns including the WNPSH, the trough over south China, and the LLJs between the two systems.

Acknowledgements

This study is supported by the Chinese 973 programme 2013CB430104 and the Chinese National Science Foundation under Grants 41330421 and 41461164006. The composite radar reflectivity mosaics were made available by the Chinese National Meteorological Center of China Meteorological Administration (CMA).

References

Augustine JA, Caracena F. 1994. Lower-tropospheric precursors to nocturnal MCS development over the Central United States. *Weather Forecast.* **9**: 116–135, doi: 10.1175/1520-0434(1994)009<0116:LTPTNM>2.0.CO;2.

Augustine JA, Howard KW. 1991. Mesoscale convective complexes over the United States during 1986 and 1987. *Mon. Weather Rev.* **119**: 1575–1589, doi: 10.1175/1520-0493(1991)119<1575:MCCOTU>2.0.CO;2.

Bartels DL, Maddox RA. 1991. Midlevel cyclonic vortices generated by mesoscale convective systems. *Mon. Weather Rev.* **119**: 104–118, doi: 10.1175/1520-0493(1991)119<0104:MCVGBM>2.0.CO;2.

Bluestein HB, Jain MH. 1985. Formation of mesoscale lines of pirecipitation: severe squall lines in Oklahoma during the spring. *J. Atmos. Sci.* **42**: 1711–1732.

Chen SJ, Lee DK, Tao ZY, Kuo YH. 1999. Mesoscale convective system over the yellow sea – a numerical case study. *Meteorog. Atmos. Phys.* **70**: 185–199.

Chen G, Sha W, Iwasaki T. 2009. Diurnal variation of precipitation over southeastern China: 2. Impact of the diurnal monsoon variability. *J. Geophys. Res.* **114**: D21105, doi: 10.1029/2009JD012181.

Chen G, Sha W, Sawada M, Iwasaki T. 2013. Influence of summer monsoon diurnal cycle on moisture transport and precipitation over eastern China. *J. Geophys. Res.* **118**: 3163–3177.

Compagnucci RH, Richman MB. 2008. Can principal component analysis provide atmospheric circulation or teleconnection patterns? *Int. J. Climatol.* **28**: 703–726.

Davis CA, Trier SB. 2002. Cloud-resolving simulations of mesoscale vortex intensification and its effect on a serial mesoscale convective system. *Mon. Weather Rev.* **130**: 2839–2858, doi: 10.1175/1520-0493(2002)130<2839:CRSOMV>2.0.CO;2.

Feng X, Liu C, Rasmussen R, Fan G. 2014. A 10-yr climatology of Tibetan plateau vortices with NCEP climate forecast system reanalysis. *J. Appl. Meteorol. Climatol.* **53**: 34–46, doi: 10.1175/JAMC-D-13-014.1.

Fritsch JM, Kane RJ, Chelius CR. 1986. The contribution of mesoscale convective weather systems to the warm-season precipitation in the United States. *J. Clim. Appl. Meteorol.* **25**: 1333–1345, doi: 10.1175/1520-0450(1986)025<1333:TCOMCW>2.0.CO;2.

Fu S-M, Zhang J-P, Sun J-H, Zhao T-B. 2016. Composite analysis of long-lived mesoscale vortices over the middle reaches of the Yangtze River valley: octant features and evolution mechanisms. *J. Clim.* **29**: 761–781, doi: 10.1175/JCLI-D-15-0175.1.

Geerts B. 1998. Mesoscale convective systems in the Southeast United States during 1994–95: a survey. *Weather Forecast.* **13**: 860–869.

Glickman TS, Zenk W. 2000. *Glossary of Meteorology*, 2nd edn. Amer. Meteor. Soc, 855 pp.

Goswami BN, Venugopal V, Sengupta D, Madhusoodanan M, Xavier PK. 2006. Increasing trend of extreme rain events over India in a warming environment. *Science* **314**: 1442–1445.

He H, Zhang F. 2010. Diurnal variations of warm-season precipitation over Northern China. *Mon. Weather Rev.* **138**: 1017–1025, doi: 10.1175/2010MWR3356.1.

Houze RA. 2004. Mesoscale convective systems. *Rev. Geophys.* **42**: RG4003, doi: 10.1029/2004RG000150.

Huang J. 1989. The significant test for meteorological element field (in Chinese). *Meteorol. Monthly* **4**: 001.

Huth R. 1993. An example of using obliquely rotated principal components to detect circulation types over Europe. *Meteorol. Z.* **2**: 285–293.

Huth R. 1996. Properties of the circulation classification scheme based on the rotated principal component analysis. *Meteorog. Atmos. Phys.* **59**: 217–233.

Huth R. 2000. A circulation classification scheme applicable in GCM studies. *Theor. Appl. Climatol.* **67**: 1–18.

Huth R, Coauthors. 2008. Classifications of atmospheric circulation patterns: recent advances and applications. *Ann. N. Y. Acad. Sci.* **1146**: 105–152, doi: 10.1196/annals.1446.019.

Jirak IL, Cotton WR, McAnelly RL. 2003. Satellite and radar survey of mesoscale convective system development. *Mon. Weather Rev.* **131**: 2428–2449.

Kunkel KE, Andsager K, Easterling DR. 1999. Long-term trends in extreme precipitation events over the conterminous United States and Canada. *J. Clim.* **12**: 2515–2527, doi: 10.1175/1520-0442(1999)012<2515:LTTIEP>2.0.CO;2.

Kyselý J, Huth R. 2005. Changes in atmospheric circulation over Europe detected by objective and subjective methods. *Theor. Appl. Climatol.* **85**: 19–36, doi: 10.1007/s00704-005-0164-x.

Laing AG, Fritsch JM. 1993. Mesoscale convective complexes in Africa. *Mon. Weather Rev.* **121**: 2254–2263.

Laing AG, Fritsch JM. 1997. The global population of mesoscale convective complexes. *Q. J. R. Meteorol Soc* **123**: 389–405.

Laing AG, Fritsch JM. 2000. The large-scale environments of the global populations of mesoscale convective complexes. *Mon. Weather Rev.* **128**: 2756–2776.

Lau K-M, Chan PH. 1983. Short-term climate variability and atmospheric teleconnections from satellite-observed outgoing longwave radiation. Part I: simultaneous relationships. *J. Atmos. Sci.* **40**: 2735–2750.

Lewis MW, Gray SL. 2010. Categorisation of synoptic environments associated with mesoscale convective systems over the UK. *Atmos. Res.* **97**: 194–213.

Liu H-B, Li L-J, Wang B. 2012. Low-level jets over southeast China: The warm season climatology of the summer of 2003. *Atmos. Oceanic Sci. Lett.* **5**: 394–400.

Ma Y, Wang X, Tao ZY. 1997. Geographic distribution and life cycle of mesoscale convective system in China and its vicinity. *Prog. Nat. Sci.* **7**: 583–589.

Maddox RA. 1980. Mesoscale convective complexes. *Bull. Am. Meteorol. Soc.* **61**: 1374–1387.

Maddox RA. 1983. Large-scale meteorological conditions associated with midlatitude, mesoscale convective complexes. *Mon. Weather Rev.* **111**: 1475–1493.

Markowski P, Richardson Y. 2010. *Mesoscale Meteorology in Midlatitudes*. John Wiley & Sons, 407 pp.

Martin JE. 1998. The structure and evolution of a continental winter cyclone. Part II: frontal forcing of an extreme snow event. *Mon. Weather Rev.* **126**: 329–348, doi: 10.1175/1520-0493(1998)126<0329:TSAEOA>2.0.CO;2.

Meng Z, Yan D, Zhang Y. 2013. General features of squall lines in East China. *Mon. Weather Rev.* **141**: 1629–1647, doi: 10.1175/mwr-d-12-00208.1.

Miller JE. 1948. On the concept of frontogenesis. *J. Meteorol.* **5**: 169–171, doi: 10.1175/1520-0469(1948)005<0169:OTCOF>2.0.CO;2.

Miller D, Fritsch J. 1991. Mesoscale convective complexes in the western Pacific region. *Mon. Weather Rev.* **119**: 2978–2992.

Panthou G, Mailhot A, Laurence E, Talbot G. 2014. Relationship between surface temperature and extreme rainfalls: a multi-time-scale and event-based analysis. *J. Hydrometeorol.* **15**: 1999–2011, doi: 10.1175/JHM-D-14-0020.1.

Parker MD, Johnson RH. 2000. Organizational modes of midlatitude mesoscale convective systems. *Mon. Weather Rev.* **128**: 3413–3436.

Peters JM, Schumacher RS. 2014. Objective categorization of heavy-rain-producing MCS synoptic types by rotated principal component analysis. *Mon. Weather Rev.* **142**: 1716–1737, doi: 10.1175/mwr-d-13-00295.1.

Philipp A, Beck C, Huth R, Jacobeit J. 2014. Development and comparison of circulation type classifications using the COST 733 dataset and software. *Int. J. Climatol.* **36**: 2673–2691, doi: 10.1002/joc.3920.

Plaut G, Simonnet E. 2001. Large-scale circulation classification, weather regimes, and local climate over France, the Alps and Western Europe. *Clim. Res.* **17**: 303–324.

Raymond DJ, Jiang H. 1990. A theory for long-lived mesoscale convective systems. *J. Atmos. Sci.* **47**: 3067–3077, doi: 10.1175/1520-0469(1990)047<3067:ATFLLM>2.0.CO;2.

Richman MB. 1986. Rotation of principal components. *J. Climatol.* **6**: 293–335.

Salio P, Nicolini M, Zipser EJ. 2007. Mesoscale convective systems over Southeastern South America and their relationship with the South American low-level jet. *Mon. Weather Rev.* **135**: 1290–1309, doi: 10.1175/mwr3305.1.

Schumacher RS, Johnson RH. 2005. Organization and environmental properties of extreme-rain-producing mesoscale convective systems. *Mon. Weather Rev.* **133**: 961–976, doi: 10.1175/MWR2899.1.

Schumacher RS, Johnson RH. 2006. Characteristics of U.S. extreme rain events during 1999–2003. *Weather Forecast.* **21**: 69–85, doi: 10.1175/WAF900.1.

Schumacher RS, Johnson RH. 2008. Mesoscale processes contributing to extreme rainfall in a midlatitude warm-season flash flood. *Mon. Weather Rev.* **136**: 3964–3986, doi: 10.1175/2008MWR2471.1.

Shi N, Gu J-Q, Huang X, Liu J, Gu Z. 2004. Significance test and Monte Carlo test used in composite analysis of window field and applications (in Chinese). *Chin. J. Atmos. Sci.* **28**: 950–956.

Shu Y, Pan Y, Wang J. 2013. Diurnal variation of MCSs over Asia and the western Pacific Region. *Acta Meteorol. Sin.* **27**: 435–445.

Sun J, Zhang X, Qi L, Zhao S. 2005a. An analysis of a meso-beta system in a Mei-yu front using the intensive observation data during CHeRES 2002. *Adv. Atmos. Sci.* **22**: 278–289.

Sun J, Zhang X, Wei J, Zhao S. 2005b. A study on severe heavy rainfall in North China during the 1990s (in Chinese). *Clim. Environ. Res.* **10**: 492–506.

Sun J, Zhao S, Xu G, Meng Q. 2010. Study on a mesoscale convective vortex causing heavy rainfall during the Mei-yu season in 2003. *Adv. Atmos. Sci.* **27**: 1193–1209, doi: 10.1007/s00376-009-9156-6.

Sun LH, Ai WX, Song WL, Wang YM. 2011. Study on climatic characteristics of china-influencing tropical cyclones. *J. Trop. Meteorol.* **17**: 181–186, doi: 10.3969/j.issn.1006-8775.2011.02.011.

Tao S-Y. 1980. *Heavy Rain in China (in Chinese)*. Chinese Science Press, 255 pp.

Velasco I, Fritsch JM. 1987. Mesoscale convective complexes in the Americas. *J. Geophys. Res.* **92**: 9591–9613.

Wang Q-W, Tan Z-M. 2014. Multi-scale topographic control of southwest vortex formation in Tibetan Plateau region in an idealized simulation. *J. Geophys. Res.* **119**: 11543–11561, doi: 10.1002/2014JD021898.

Wang Y, Zhou L. 2005. Observed trends in extreme precipitation events in China during 1961–2001 and the associated changes in large-scale circulation. *Geophys. Res. Lett.* **32**: L09707, doi: 10.1029/2005GL022574.

Wang D, Zhang Y, Huang A. 2013. Climatic features of the south-westerly low-level jet over southeast china and its association with precipitation over east China. *Asia-Pac. J. Atmos. Sci.* **49**: 259–270, doi: 10.1007/s13143-013-0025-y.

Wang C-C, Chieh-Sheng Hsu J, Tai-Jen Chen G, Lee D-I. 2014. A study of two propagating heavy-rainfall episodes near Taiwan during SoWMEX/TiMREX IOP-8 in June 2008. Part I: Synoptic evolution, episode propagation, and model control simulation. *Mon. Weather Rev.* **142**: 2619–2643.

WMO. 1992. International meteorology vocabulary. WMO/OMN/BMO Report No. 182, World Meteorological Organization: Geneva, Switzerland.

Woodley WL, Olsen AR, Herndon A, Wiggert V. 1975. Comparison of gage and radar methods of convective rain measurement. *J. Appl. Meteorol.* **14**: 909–928, doi: 10.1175/1520-0450(1975)014<0909:COGARM>2.0.CO;2.

Yu Z-Y, He L-F, Fan G-Z, Li Z-C, Su Y-L. 2011. The basic features of the severe convection at the background of cold vortex over North China. *J. Trop. Meteorol.* **1**: 009.

Zhai P, Zhang X, Wan H, Pan X. 2005. Trends in total precipitation and frequency of daily precipitation extremes over China. *J. Clim.* **18**: 1096–1108, doi: 10.1175/JCLI-3318.1.

Zhao Y, Zhang Q, Du Y, Jiang M, Zhang J. 2013. Objective analysis of circulation extremes during the 21 July 2012 torrential rain in Beijing. *Acta Meteorol. Sin.* **27**: 626–635.

Zheng YG, Tao ZY, Wang HQ, Lee DK. 1999. Environment of meso-alpha-scale convective system development in Yellow Sea region. *Prog. Nat. Sci.* **9**: 842–848.

Zheng Y, Chen J, Zhu P. 2008a. Climatological distribution and diurnal variation of mesoscale convective systems over China and its vicinity during summer. *Chin. Sci. Bull.* **53**: 1574–1586.

Zheng Y, Chen J, Ge G, Huang Y, Zhang C. 2008b. Review on the synoptic scale Mei-yu front system and its synoptics' definition (in Chinese). *Acta Sci. Nat. Univ. Pekinensis.* **44**: 157–164.

Zheng L, Sun J, Zhang X, Liu C. 2013. Organizational modes of mesoscale convective systems over central East China. *Weather Forecast.* **28**: 1081–1098, doi: 10.1175/waf-d-12-00088.1.

